Inorganica Chimica Acta 441 (2016) 67–77

Contents lists available at ScienceDirect

Inorganica Chimica Acta

journal homepage: www.elsevier.com/locate/ica

Energy transfer process in highly photoluminescent binuclear hydrocinnamate of europium, terbium and gadolinium containing 1,10-phenanthroline as ancillary ligand

Lippy F. Marques [a,*], Alexandre Cuin [b], Gustavo S.G. de Carvalho [b], Molíria V. dos Santos [c], Sidney J.L. Ribeiro [c], Flávia C. Machado [b]

[a] Instituto de Química, Universidade do Estado do Rio de Janeiro, Rio de Janeiro 20550-013, Brazil
[b] Departamento de Química-ICE, Universidade Federal de Juiz de Fora, Juiz de Fora, MG 36036-330 Brazil
[c] Instituto de Química, Universidade Estadual Paulista Júlio de Mesquita Filho, UNESP, Araraquara, SP 14801-970, Brazil

ARTICLE INFO

Article history:
Received 14 September 2015
Received in revised form 3 November 2015
Accepted 5 November 2015
Available online 14 November 2015

Keywords:
Hydrocinnamic acid
Photoluminescence studies
Nitrogen ligands

ABSTRACT

New binuclear lanthanide (III) complexes of general formula $[Ln_2(hcin)_6(phen)_2]$ (where Ln = Eu **1**; Gd **2**; Tb **3**; hcin = hydrocinnamate anion; phen = 1,10-phenanthroline) were synthesized and fully characterized by elemental analysis, vibrational spectroscopy (infrared and Raman), thermal analysis (TGA/DTA), CP/MAS ^{13}C NMR and powder X-ray diffraction. The crystal description based on powder X-ray diffraction data reveals that all compounds are isostructural and that each lanthanide ion is nine coordinated by oxygen and nitrogen atoms to form distorted tricapped trigonal-prismatic coordination polyhedron. The photoluminescence behavior was studied based on the excitation and emission spectra and luminescence decay curves. The emission spectra of Eu(III) and Tb(III) complexes are composed of intense and typical red and green emissions, respectively. Phosphorescence data of Gd(III) complex showed that the triplet states (T_1) of ligands have higher energy than the main emitting states of Eu(III) and Tb(III) indicating the possibility of intramolecular energy transfer for these metal ions. To elucidate the energy transfer process in the Eu(III) complex, spectroscopic properties as Ω_λ intensity parameters ($\lambda = 2$ and 4), radiative (A_{rad}) and nonradiative (A_{nrad}) decay rates and quantum efficiency (η) of $[Eu_2(hcin)_6(phen)_2]$ were determined. Such spectroscopic properties were compared with $[Eu_2(hcin)_6(bpy)_2]$ complex properties recently reported. The high emission quantum efficiency ($\eta = 72\%$) for Eu(III) complex **1** showed that it is a potential candidate as emitter in photonic systems.

1. Introduction

The chemistry and spectroscopy of lanthanide ions (Ln(III)) differ considerably from *d*-shell transition metal ions. The shielding of *4f* orbitals by the filled $5p^6 6s^2$ subshells results in special optical features of lanthanide ions such as the minimal perturbation by the external field generated by the ligands [1,2]. For example, lanthanide compounds are characterized as exhibiting narrow line-like emissions of optical pure colors. All lanthanide ions, except La(III) and Lu(III) are luminescent, but the investigation of Eu(III) and Tb(III) ions luminescence properties has a special relevance because their specific strong red (~615 nm) and green (~540 nm) emission, and also the long lifetimes of the excited $^5D_0$ and $^5D_4$ states, respectively. In this case, it is not surprising that these compounds are currently applied in different fields, ranging from light emitting diodes to enable full-color and low-cost to fluoroimmunoassay reagents [3–5]. The search of new lanthanide complexes has been an active area of research in coordination chemistry mainly due to the possibility of designing novel photoluminescent materials [6–8]. However, the use of some lanthanide ions systems with direct absorption of the *f* excited states is very inefficient because the *f–f* transitions are parity forbidden, resulting in very low absorption coefficients. In order to overcome this drawback, suitable chromophores have been employed as antennas (or sensitizers) that have the capability of transferring energy indirectly to lanthanide ions [9]. In general, the choice of the ligand is important for the emission efficiency and in particular several chromophoric antenna ligands, like β-diketonate [10,11] and carboxylate ligands [12–14], collect the photons and transfer their energy towards the lanthanide center which gets indirectly excited and emits light during the relaxation process. In particular, the

* Corresponding author. Tel.: +55 21 23340563.
E-mail address: lippymarquesuerj@gmail.com (L.F. Marques).

http://dx.doi.org/10.1016/j.ica.2015.11.009
0020-1693/

hydrocinnamic acid (Hhcin) or 3-phenylpropanoic acid is an analog of phenylalanine [15] and belongs to the class of phenylpropanoids used as additives in food and pharmaceuticals products [16]. Despite its structural simplicity, there are very few studies of complexes with the hydrocinnamic acid [17–20]. In addition, previous studies show that the emission intensities and fluorescence lifetimes of lanthanide complexes are enhanced after introducing the second organic ligand as 2,2′-bipyridine (bpy) or 1,10-phenanthroline (phen) [20–22]. These ligands act as energy donors and enhance the fluorescence intensities of lanthanide complexes in a so-called "*synergistic effect*". The introduction of these ligands not only reinforces the fluorescence emission, but also increases the thermal stability and fulfills the coordination numbers of lanthanide complexes. In the present paper we report the one-step synthesis, structural characterization and photoluminescence study of three new binuclear lanthanide (III) complexes *[Ln_2(hcin)$_6$(phen)$_2$]* (Ln = Eu **1**; Gd **2**; Tb **3**; hcin = hydrocinnamate anion; phen = 1,10-phenanthroline). Photoluminescence data were obtained from the excitation, emission spectra and luminescence decay curves. The energy transfer process from the excited states of ligands to the intraconfigurational states of the Ln(III) ions was also investigated. Spectroscopic properties as Ω_λ intensity parameters (λ = 2 and 4), radiative (A_{rad}) and nonradiative (A_{nrad}) decay rates and quantum efficiency (η) of *[Eu_2(hcin)$_6$(phen)$_2$]* were determined and compared with those for the complex *[Eu_2(hcin)$_6$(bpy)$_2$]* recently reported [20].

2. Experimental

2.1. Materials and measurements

All synthetic procedures were performed in air and $TbCl_3{\cdot}6H_2O$, hydrocinnamic acid (Hhcin) and 1,10-phenanthroline (phen) were obtained either from Aldrich® or Fluka® and used as received. $EuCl_3{\cdot}6H_2O$ and $GdCl_3{\cdot}6H_2O$ were prepared by dissolving europium and gadolinium oxide in hydrochloric acid solution and then dried. Elemental analyses for C, H and N were carried out using a Perkin-Elmer 2400CHN analyzer. FTIR spectra were recorded with a Perkin Elmer (Spectrum One model) FTIR spectrophotometer using KBr pellets in the wavenumber range of 4000–400 cm^{-1} with an average of 128 scans and 4 cm^{-1} of spectral resolution. Fourier-Transform Raman spectroscopy was carried out using a Bruker RFS 100 instrument, Nd^{3+}/YAG laser operating at 1064 nm in the near-infrared and CCD detector cooled with liquid N_2. Good signal-to-noise ratios were obtained from 2000 scans accumulated over a period of about 30 min, using 4 cm^{-1} as spectral resolution. Thermal analysis (TG and DTA curves) were obtained on a Shimadzu TG-60 equipment where about 6–10 mg of samples were heated at 10 °C/min from room temperature to 800 °C in a dynamic argon atmosphere (flow rate = 100 mL/min). The CP/MAS ^{13}C NMR experiments were performed on a Bruker Avance III HD 300 spectrometer (7.04 T), operated at a Larmor frequency of 75.00 MHz. The analyses were performed on a MAS probe in ZrO_2 rotors (and Kel-F caps) of 4 mm. The spectra were obtained using MAS, at a frequency of 10000 Hz, and cross polarization. The chemical shifts were indirectly standardized on a sample of glycine with respect to the carbonyl signal at 176.00 ppm relative to TMS which is the primary standard. The luminescence excitation and emission spectra were recorded using a Jobin–Yvon Model Fluorolog FL3-22 spectrophotometer equipped with a R928 Hamamatsu photomultiplier and 450 W xenon lamp as excitation source and the spectra were corrected with respect to the Xe lamp intensity and spectrometer response. Measurements of emission decay were performed with the same equipment by using a pulsed Xe (3 μs bandwidth) source.

2.2. X-ray powder diffraction data collection and structure determination

To perform the full powder X-ray diffraction analysis the three polycrystalline lanthanides complexes were gently grounded in an agate mortar. Then, the powder of each compound was deposited in the hollow of very thin glass sample holder which has nearly zero background plate. The X-ray diffraction data were collected by overnight scans in the 2θ range of 7–105° with steps of 0.02° and 0.5 s per step using a *Bruker AXS D8 da Vinci* diffractometer, equipped with Ni-filtered CuKα radiation (λ = 1.5418 Å) and a Lynxeye linear position-sensitive detector. The following optics were set up: primary beam Soller slits (2.94°), fixed divergence slit (0.3°) and receiving slit (8 mm). The generator was set at 40 kV and 40 mA. Approximate unit cell parameters were determined using 20 first standard peaks, followed by indexing through the single-value decomposition approach [23] implemented in TOPAS [24]. In all cases, space group $P2_1/n$ was chosen after careful analysis of systematic absences and the cell parameters were refined using 7–55 2θ range by Pawley method [25]. The successful structure solution processes were performed by the simulated annealing technique [26] also implemented in TOPAS. No higher symmetric system was suggested by PLATON [27]. The structure solution of each complex was carried out using four full rigid bodies, being one for neutral phen ligand and three for the anionic hcin ligands, all of them with free location and orientation and three refinable torsion angles (τ_1, τ_2, τ_3,) for hcin anions, see Chart 1. Rigid bodies of ligands were defined by the Z-matrix formalism using standard distances and angle bonds already reported in literature [28,29]. Ln(III) ions (Ln = Eu, Gd and Tb) were also left free in translation. It is worth noting that in the structure solution step there are 36 parameters to be determined and it is the beyond of powder X-ray diffraction state-of-art. However, using some soft restrains as Eu–O below than 2.8 Å, feasible and robust crystallographic models were afforded in this step after some hours of computation procedures.

In all cases, the final crystal model refinements afforded in former step were carried out by the well-known Rietveld method [30] where the rigid body description introduced at the solution stage was maintained, but without any restrains. The background was modeled by a Chebyshev polynomial function. Isotropic thermal parameters set up as 3.3 (0.1) Å^2 for **1**, 0.95 (0.1) Å^2 for **2** and 2.7 (0.1) Å^2 for **3** were assigned to all atoms. A summary of crystal data and data collection parameters are presented in Table 1. The final Rietveld refinement plots are supplied as Supplementary Materials S1–S3 for **1**, **2** and **3** complexes, respectively.

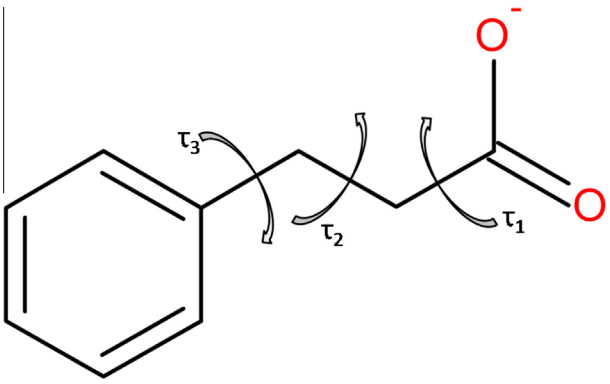

Chart 1. Sketch of hydrocinnamate-hcin ion. The τ_1 to τ_3 illustrate the torsion angles defining the conformation of the organic moiety in describing the full conformation of the whole ligand.

Table 1
Main crystallographic data of *[Ln$_2$(hcin)$_6$(phen)$_2$]* complexes.

	1 *[Eu$_2$(hcin)$_6$(phen)$_2$]*	**2** *[Gd$_2$(hcin)$_6$(phen)$_2$]*	**3** *[Tb$_2$(hcin)$_6$(phen)$_2$]*
Empirical formula	$Eu_2(C_9H_9O_2)_6(C_{12}H_8N_2)_2$	$Gd_2(C_9H_9O_2)_6(C_{12}H_8N_2)_2$	$Tb_2(C_9H_9O_2)_6(C_{12}H_8N_2)_2$
Formula weight	1559.34	1569.92	1573.26
T (K)	295	295	295
λ (Cu Kα) (Å)	1.5418	1.5418	1.5418
Crystal system	monoclinic	monoclinic	monoclinic
Space group	$P2_1/n$	$P2_1/n$	$P2_1/n$
a (Å)	13.551(3)	13.530(4)	13.507(4)
b (Å)	22.355(4)	22.340(6)	22.346(6)
c (Å)	12.333(3)	12.316(4)	12.301(4)
β (°)	66.14(2)	66.12(2)	66.09(2)
V (Å^3)	3416.9(1)	3304.1(2)	3394.0(2)
Z	4	4	4
D_{calc} (g/cm^3)	1.516	1.532	1.539
μ (mm^{-1})	12.27	12.98	10.27
F(000)	1632	1640	1644
Number of parameters	59	54	53
R_{Bragg}, R_{wp}	0.022/0.033	0.024/0.030	0.019/0.032

2.3. Synthesis of *[Ln$_2$(hcin)$_6$(phen)$_2$]*

An ethanolic solution (10 mL) containing 24 mg (0.13 mmol) of 1,10-phenanthroline was slowly added to an aqueous suspension (30 mL) containing 60 mg of Hhcin (0.40 mmol), 50 mg of $LnCl_3 \cdot 6H_2O$ (0.13 mmol) and NaOH aqueous solution (0.40 mL, 1 mol L^{-1}). The mixture was stirred at room temperature for 24 h and a white solid was formed. The solid was filtered, washed three times with ethanol and acetone and dried in air.

[Eu$_2$(hcin)$_6$(phen)$_2$] (***1***): Yield: 73%. *Anal.* Calc. for $C_{78}H_{70}O_{12}N_4Eu_2$: C, 60.08; H, 4.52; N, 3.59. Found: C. 59.8; H, 4.51; N, 3.63%.

[Gd$_2$(hcin)$_6$(phen)$_2$] (***2***): Yield: 74%. *Anal.* Calc. for $C_{78}H_{70}O_{12}N_4Gd_2$: C, 59.6; H, 4.49; N, 3.57. Found: C. 59.4; H, 4.49; N, 3.64%.

[Tb$_2$(hcin)$_6$(phen)$_2$](***3***): Yield of 77%. *Anal.* Calc. for $C_{78}H_{70}O_{12}N_4Tb_2$: C, 59.5; H, 4.48; N, 3.56%. Found: C, 60.2; H, 4.47; N, 3.59%.

All the compounds are stable in air and exhibited intense luminescence in the primary colors: red (for the compound **1**) and green (for the compound **3**), when exposed to UV light.

Our research group has some experience on solvothermal synthesis and crystal structures, and recently binuclear hydrocinnamates of Eu(III), Gd(III) and Tb(III) of general formula *[Ln$_2$(hcin)$_6$(bpy)$_2$]*, similar to those studied here, were reported [20]. In this sense, several efforts have been made, including solvothermal synthesis, to obtain single crystals for structural determination through single crystal X-ray diffraction analysis. Fortunately, the obtained solids were crystalline powders and we also have same expertise in solving crystal structures using powder X-ray diffraction (PXRD) data [31–33]. Therefore, in absence of single crystals, the crystallographic models of present lanthanides complexes were provided by PXRD studies and once again, it has been shown that this method can supply relevant and otherwise inaccessible structural information that can be obtained from single crystal analyses [34].

3. Results and discussion

All the new complexes described here were confirmed by satisfactory elemental analysis, vibrational spectroscopy (infrared and Raman), CP/MAS ^{13}C NMR, thermal analysis (TG/DTA), X-ray diffraction and photoluminescence study.

From the reaction between $LnCl_3 \cdot 6H_2O$ (Ln = Eu, Gd and Tb), hydrocinnamic acid (Hhcin) and 1,10-phenanthroline (phen) in 1:4:1 molar quantities, using the conventional agitation method, compounds of general formula *[Ln$_2$(hcin)$_6$(phen)$_2$]* were obtained. Elemental analysis data of C, H and N indicates the (1:3:1)/(Ln(III):hcin:phen) stoichiometric proportion that is not the same used in the synthetic procedure.

3.1. Crystal Structures of *[Ln$_2$(hcin)$_6$(phen)$_2$]*

Powder X-ray diffraction analysis reveals that the three lanthanides complexes belong to monoclinic system and space group $P2_1/n$. Since the complexes are isostructural (see Figs. S1–S3 in Supplementary Material), the crystal structure of Eu(III) complex was chosen to be described herein as a representative example. The asymmetric unit of Eu(III) complex is shown in Fig. 1(a) and in Fig. 1(b) is possible to see that the crystal structure, in fact, consists of a discrete dimeric neutral molecule, with molecular formula *[Eu$_2$(hcin)$_6$(phen)$_2$]*. It is interesting to observe that the dimeric system of Eu(III) complex has an inversion center of symmetry located between two Eu(III) ions indicating that the Eu(III) ions are both equivalent in the coordination environment. Eu(III) ions are surrounded by seven oxygen atoms from hydrocinnamate ligands and two nitrogen atoms from phenanthroline ligand completing the coordination number nine. The coordination geometry of Eu(III) is well described as a distorted tricapped trigonal prism (Fig. 1c). The main lengths bonds found in Ln(III) complexes are listed in Table 2.

The carboxylate groups from three crystallographically independent hcin ligands present three different coordination modes as can see in Chart 2. Carboxylate oxygen atoms can act as bidentate chelating, Chart 2(a), and, one of the oxygen atoms O (or O*i*) is coordinated to another Ln(III) ion forming a monoatomic bridge or μ-oxo bridge. The carboxylate group can also connect a pair of Eu (III) ions in a *syn,syn-*η^1:η^1:μ_2 bidentate bridging fashion, as depicted in Chart 2(b), In coordination mode (c), hcin acts as simple bidentate chelating ligand toward one Eu(III) center with two oxygen atoms from carboxylate group.

Besides the Ln–N and Ln–O lengths, an important value is the distance of Ln···Ln ions. For **1**, Eu(III)···Eu(III)^i distance is 4.063 Å and it is slightly larger than in **2** with Gd(III)···Gd(III)^i distance of 4.032 Å. As expected the Tb(III)···Tb(III)^i distance, about 3.992 Å, is slightly shorter than in **1** and **2** since their ionic radii are 0.95 Å Eu(III) versus 0.94 Å Gd(III) vs 0.92 Å Tb(III). Based on the literature [20], Ln–N and Ln–O bond lengths are about 2.6 and 2.4 Å, respectively, and Ln–N and Ln–O distances in compounds **1**–**3** vary from 2.59 to 2.75 and from 2.38 to 2.79 Å (see Table 2).

As discussed previously [20], lanthanide complexes of monoacids can form coordination polymers with bridging carboxylate groups including cinnamate [36], nitrobenzoate [37], 2,3-dimethoxybenzoates [38] and 2-thiopheneacetate [39]. On

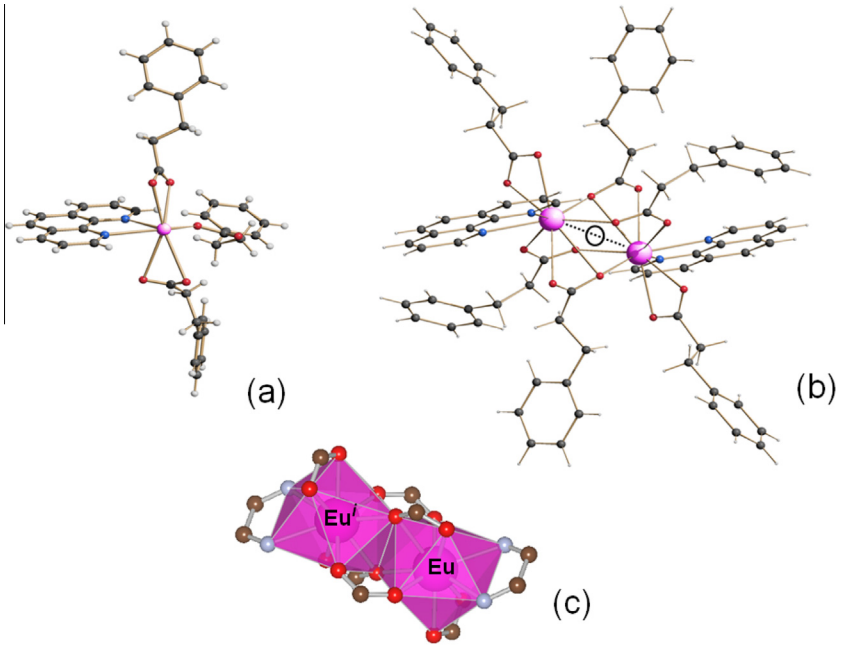

Fig. 1. Asymmetric unit of compound **1** (a) and its dimer complex *[Eu$_2$(hcin)$_6$(phen)$_2$]* (b) drawn using SCHAKAL [35] Color codes: C, dark-gray; H, light-gray, O, red; N, blue and Eu, pink. The inversion center, highlighted in (b) by a circle, is centered between two Eu(III) ions and all atoms of dimer were generated applying inversion symmetric code. Polyhedra formed by [EuO$_6$N$_2$] units are shown in (c) and they are connected through cin anions. (For interpretation of the references to color in this figure legend, the reader is referred to the web version of this article.)

Table 2
Selected values of bond distances of the Ln(III) complexes **1**, **2** and **3.**

Complex	Ln···Ln^i	Ln–N	Lengths (Å) Ln–O and Ln^i–O		
			Mode (a)	Mode (b)	Mode (c)
1	4.063	2.593(2)	2.776(1)	2.385(2)^i	2.515(3)
		2.747(1)	2.497(1)	2.499(3)	2.480(4)
			2.492(1)^i		
2	4.032	2.688 (1)	2.708(2)	2.541(1)^i	2.499(1)
		2.609(1)	2.555(1)	2.459(1)	2.511(2)
			2.478(1)^i		
3	3.992	2.621(7)	2.696(1)	2.588(8)	2.487(1)
		2.587(8)	2.583(1)	2.543(1)	2.488(1)
			2.542(1)^i		

Symmetry code $i = 2 - x, 1 - y, 1 - z$.

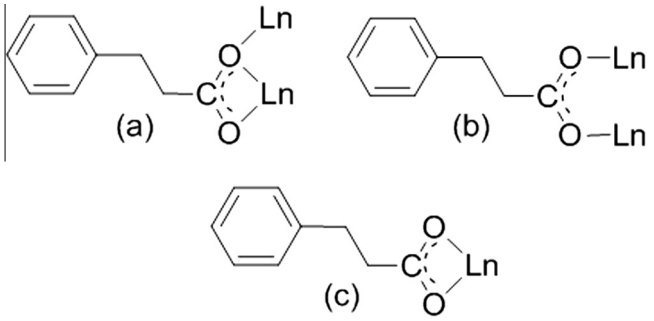

Chart 2. Three possible coordination modes of hydrocinammate ion.

the other hand, dimeric complexes can be achieved when carboxylate ligands along with 2,2′-bipyridine (bpy) or 1,10-phenanthroline (phen) are used as exemplified by *{[Eu$_2$(2-BrBA)$_6$(bpy)$_2$]$_2$·CH$_3$CH$_3$OH·H$_2$O}*[54] (2BrBA = 2-bromobenzoate) and *[Eu$_2$(3,4-DMBA)$_6$(phen)$_2$]*[55] (3,4-DMBA = 3,4-dimethylbenzoate). Results on the synthesis and crystal structures of complexes with hydrocinnamate anion are unusual [25,26]. However, our group has reported the first crystal structures of lanthanide hydrocinnamates [19,20], and to the best of our knowledge, these are still the first structures these compounds. A supramolecular one-dimensional (1D) array along *c* axis has been built by weak non-classical hydrogen bonds (CH···O) between the oxygen atom from carboxylate group and aromatic ring CH groups from the phen ligands d(C65···O21) = 3.364 Å as well CH from cin-d(C34···O22) = 3.828 Å as shown in Fig. 2. Other hydrogen bonds between C12–O11 are responsible for the formation of a supramolecular network along *a* and *b* axes, and together with hydrogen bonds on c axis, a 3D network has been created. Although these interactions are weaker than those of the coordinative bonds, they play an essential role in the construction of multi-dimensional networks in the solid state, as in the present case.

3.2. Vibrational spectroscopy (infrared and Raman)

The infrared and Raman spectra of all ligands and complexes were investigated in this work. The similarity of lanthanide complexes IR and Raman spectra indicates that these compounds are isostructural, as have been proved by X-ray diffraction analysis results. The main vibrational modes are summarized in Table 3, as well as the tentative assignment.

Particular attention was paid to the separation between asymmetric and symmetric stretching frequency values of COO$^-$ groups. In this class of compounds, the difference ($\Delta\nu$) between ν_{asym}(COO$^-$) and ν_{sym}(COO$^-$) in comparison to the corresponding values in ionic species is currently employed to propose the carboxylate group coordination mode [40]. This is an important tool, since lanthanoid carboxylates usually contain a variety of different coordination modes as a result of their large coordination numbers. In the IR spectrum of hcin$^-$ ligand in ionic form Nahcin, two absorption bands at 1553 and 1418 cm^{-1} are attributed to ν_{asym}(COO$^-$) and ν_{sym}(COO$^-$) stretching modes, respectively, providing $\Delta\nu$ = 135 cm^{-1}. The FTIR and Raman spectra of the complexes show a band attributed to ν_{asym}(COO$^-$) vibrational mode at

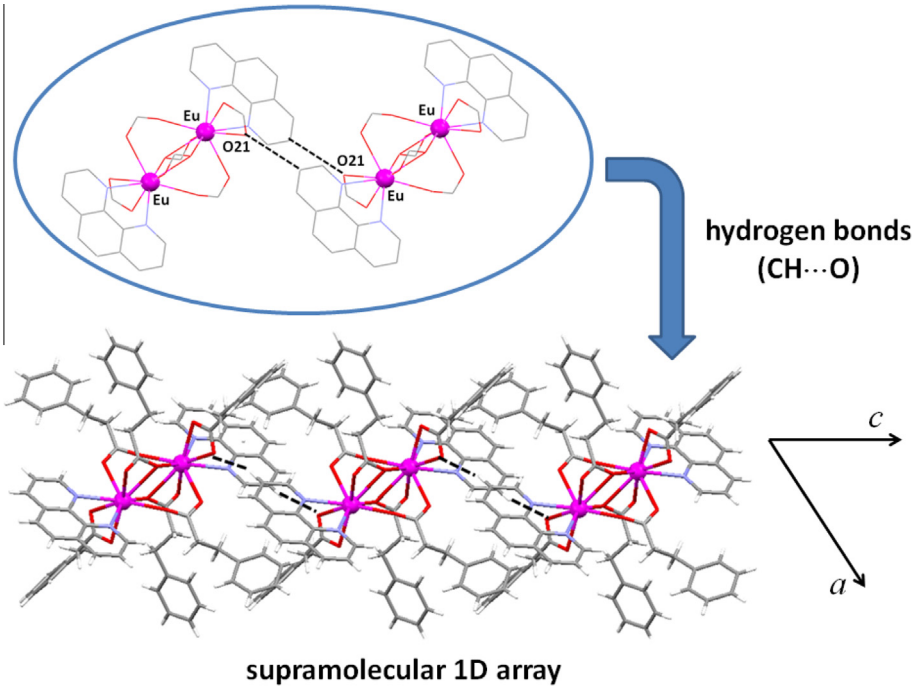

Fig. 2. The supramolecular 1D net of **(1)** complex where the CH···O hydrogen bonds were highlighted. The emphasis of core metal center of two dimer molecules is shown as inset.

Table 3
Infrared (IR) and Raman (R) wavenumbers (in cm^{-1}) and tentative assignment of the most important bands for ligands (Nahcin and 1,10-phen) and **1**–**3** complexes.

Nahcin		1,10-phen		**(1)**		**(2)**		**(3)**		Assignment
IR	R	IR	R	IR	R	IR	R	IR	R	
–	–	–	–	475 (w)	473 (w)	475 (w)	473 (w)	475 (w)	473 (w)	ν(Ln–N)
–	–	–	–	545 (w)	548 (w)	545 (w)	548 (w)	545 (w)	548 (w)	ν(Ln–O)
825 (w)	819 (w)	856 (s)	857 (w)	845 (m)	–	845 (m)	–	845 (m)	–	$\delta_{o,p}$(CH)
–	–	1598 (m)	1598 (m)	1606 (vs)	1606 (m)	1606 (vs)	1606 (m)	1606 (vs)	1606 (m)	ν(C=N)
1418 (vs)	1416 (vs)	–	–	1421 (vs)	1421 (vs)	1421 (vs)	1421 (vs)	1421 (vs)	1421 (vs)	$\nu_{sym}(COO^-)$
1553 (s)	1552 (s)	–	–	1521 (w)	1521 (w)	1521 (w)	1521 (w)	1521 (w)	1521 (w)	$\nu_{asym}(COO^-)$
2922 (s)	2917 (s)	2986 (w)	2992 (w)	2919 (w)	2917 (s)	2919 (w)	2917 (s)	2919 (w)	2917 (s)	$\nu(CH)_{aliph.}$
3032 (m)	3030 (m)	3064 (w)	3058 (m)	3021 (w)	3030 (s)	3021 (w)	3030 (s)	3021 (w)	3030 (s)	$\nu(CH)_{atom.}$

Abbreviations: vs, very strong; s, strong; m, medium; w, weak; o.p, out-of-plane; asym, asymmetric; sym, symmetric; aliph, aliphatic; arom, aromatic.

1521 cm^{-1}, while the $\nu_{sym}(COO^-)$ appears in 1421 cm^{-1}. The calculated value of $\Delta\nu$ = 100 cm^{-1} is close to the value expected for a chelate coordination mode of the carboxylate moiety, in agreement with by X-ray diffraction analysis results. Additionally, the absorption at 1598 cm^{-1} of the C=N stretching frequencies in the free phen spectrum are shifted to higher wavenumbers (1606 cm^{-1}) in *[Ln_2(hcin)$_6$(phen)$_2$]* complexes. This indicates the nitrogen ligand coordination to the lanthanide centers through the pyridine nitrogen atom, as observed for previous structurally characterized compounds containing pyridil rings [20].

3.3. Thermal analysis

Thermal behavior, particular stability and volatility, is important for practical applications in luminescent materials. The thermal analysis (TGA/DTA) was carried out using **1**–**3** polycrystalline samples in the temperature range of 19–800 °C under argon atmosphere. Because complexes **1**–**3** are isomorphous, their TGA curves are similar (Fig. S4 in Supplementary Material). Therefore only complex **3** will be discussed in detail as a representative compound for this group. As can be seen in TG/DTA curves (Fig. 3), the compound is stable up to 238 °C, indicating the absence of water molecules in its structure. The first endothermic event centered at 228 °C is probably related to the melting point for the complex. After the fusion of complex, three consecutive exothermic events

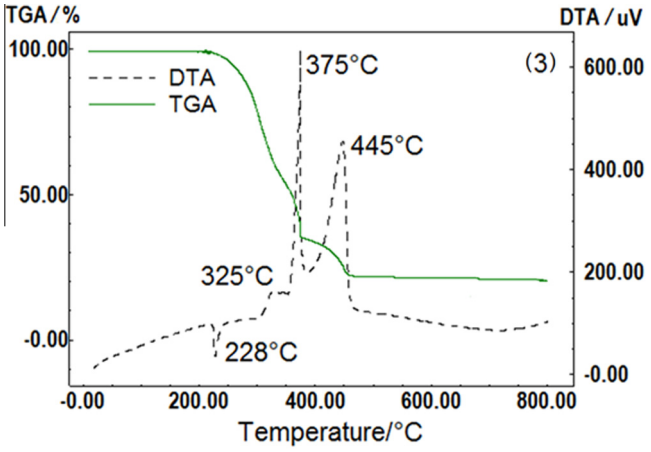

Fig. 3. TGA (—) and DTA (----) traces in Ar atmosphere for compound **3**.

occur (centered at: 325, 375 and 445 °C) which are related to consecutive thermal decomposition steps. The first one, between 238 and 313 °C, corresponds to the release of two phen ligands (Obsd: 22.0%, Calcd: 22.8%). The second and third mass losses, observed from 313 to 459 °C, are consistent with the decomposition of approximately six hydrocinnamate ligands (Obsd: 55.1%, Calcd: 56.8%). At 800 °C, the residual percentage weight is consistent with half a mol of Tb_4O_7 (Obsd. 22.9%, Calcd: 23.7%).

3.4. CP/MAS ^{13}C NMR spectra analysis

The CP/MAS ^{13}C NMR spectra of complex **1** and Hhcin and phen ligands are shown in Fig. S5 in Supplementary Material. Through the analysis of complex **1** spectrum, signals between d 24.4 and 34.0 ppm, attributed to methylene carbons of hcin ligand were observed. The presence of four signals in this region indicates different hcin ligands in the complex **1** structure, which is in accordance with vibrational spectroscopy (infrared and Raman) and PXRD analysis. The signals between δ 91.8 and 156.3 ppm were attributed to aromatic carbons from phen and hcin structure. The spectrum of complex **1**, in comparison with the ligands spectra shows a shielding of some aromatic carbons, more precisely, the peaks between δ 90.0 and 105.0 ppm. Probably, this is due to the HALA Effect (Heavy Atom on the Light Atom Effect), where a heavy atom, Eu(III) in this case, induces a shielding (or deshielding) on close light nuclei [41]. Finally, the signal around δ 210.0 ppm refers to the carboxylate carbon which appears deshielding when compared with the free Hhcin ligand spectrum, because of the decreasing on electron density, as a result of the complex formation.

Unfortunately, it was not possible to obtain CP/MAS ^{13}C NMR spectra of Gd(III) and Tb(III) complexes, probably due to their large paramagnetic effect [42], since the cross-polarization technique is susceptible to signal loss in the presence of paramagnetic species [42,43]. In addition, lanthanides may influence the relaxation time, also inducing the NMR signal loss.

3.5. Photoluminescence study

3.5.1. Phosphorescence of the Gd(III) complex

The corresponding gadolinium complex was used as a model complex for the determination of the first triplet state energies of the organic ligands ($T_1 \rightarrow S_0$ transitions) owing to their high phosphorescence/fluorescence ratio compared to those of other Ln(III) complexes and because of their structural similarity with Eu(III) and Tb(III) complexes. The Gd(III) complexes are proper for this determination due to the high energy gap (approximately 32,000 cm^{-1}) between the ground ($^8S_{7/2}$) and excited ($^6P_{7/2}$) levels within the $4f^7$ configuration which avoids the energy transfer from the ligand triplet to the metal excited levels. In this context, the larger probability of ligand phosphorescence is due to a combination of both paramagnetic [44] and heavy-atom effects [45]. The steady-state phosphorescence spectrum of gadolinium complex recorded at liquid nitrogen temperature from 385 to 480 nm with excitation at 330 nm is shown inset in Fig. 4. This spectrum is characterized by one very low intensity broad band in the spectral range of 380–450 nm and the strongest band which are assigned to $S_0 \rightarrow S_1$ (fluorescence band) and to $T_1 \rightarrow S_0$ (phosphorescence band) transitions of the ligands, respectively. This behavior has been observed for other lanthanide carboxylate complexes reported in the literature [20]. The phosphorescence band extends to longer wavelengths values presenting a high intensity due to an efficient energy transfer process to Eu(III) ion. This fact is caused by natural percentage of europium contained in gadolinium oxide used to synthesize the compound *[$Gd_2(hcin)_6(phen)_2$]*. In order to determine unequivocally the energy due to the 0–0 phonon transition for the Gd(III) complex, the time-resolved spectrum (Fig. 4) was recorded at liquid nitrogen temperature with the excitation and emission monitored at 330 and 495 nm, respectively, using 1.0 ms delay. In this case, the fluorescence bands decrease very fast as the flash delay is increased and only the phosphorescence spectrum from the ligands is displayed. As can be seen, this spectrum presents only a broad band that may be attributed to the triplet to singlet transition. The lowest ligand T_1 state energy was determined as the shortest wavelength phosphorescence band (0–0 phonon transition) for the complex *[$Gd_2(hcin)_6(phen)_2$]* and appears at approximately 451 nm (22,172 cm^{-1}). So, the high emission intensity observed for the *[$Eu_2(hcin)_6(phen)_2$]*and *[$Tb_2(hcin)_6(phen)_2$]* complexes can be explained by an efficient antenna effect with this triplet state having higher energy than the main emitting states of Eu(III) ($^5D_0$) and Tb(III) ($^5D_4$), indicating the possibility of intramolecular energy transfer for these ions.

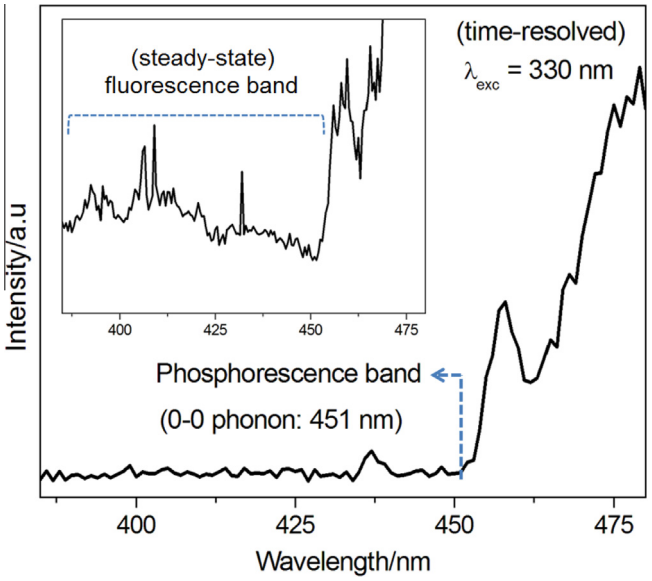

Fig. 4. Time-resolved luminescence spectrum of Gd(III) complex in solid state at 77 K, upon excitation at 330 nm. (Inset: Phosphorescence data using the steady-state technique).

3.5.2. Photoluminescence of *[$Ln_2(hcin)_6(phen)_2$]* (Ln = Eu(III) ***(1)*** and Tb(III) ***(3)***)

Fig. 5a shows the excitation spectrum of the *[$Eu_2(hcin)_6(phen)_2$]* **1** recorded at 303 K in the 250–500 range by monitoring the Eu(III) emission at 616 nm. This spectrum exhibits a broad band between 250 and 360 nm which is attributable to the ligand centered $S_0 \rightarrow S_1$ (π, π^*) transition of the aromatic moiety or with a possible charge transfer (LMCT). The absorption bands are originated from the $^7F_0$ ground state to the excited levels ^5L_J: $^5G_6$ (363 nm), $^5H_4$ (379 nm), $^5L_7$ (385 nm), $^5L_6$ (394 nm), $^5D_3$ (415 nm) and $^5D_2$ (464 nm) excited states. The $^7F_0 \rightarrow {}^5L_6$ transition exhibits the highest absorption intensity among the $4f^6$ intraconfigurational transitions of Eu(III) ion, indicating that this transition is more efficient for the direct excitation in this metal center. However, these transitions are less intense than those attributable to the ligands levels, which proves that luminescence sensitization is more efficient than the direct excitation of the Eu(III) ion absorption levels.

The emission spectrum of Eu(III) complex, showed in Fig. 5b, provides a lot of information about the point symmetry the Eu (III) ion [46]. Complex **1** exhibits several characteristic emission bands $^5D_0 \rightarrow {}^7F_J$ (J = 0–4) upon excitation in the ligand absorption band, at 330 nm. The presence of the $^5D_0 \rightarrow {}^7F_0$ transition indicates that Eu(III) ion may be located at a symmetry site of the type C_s, C_n or C_{nv}, as the selection rules for the electric dipole transition

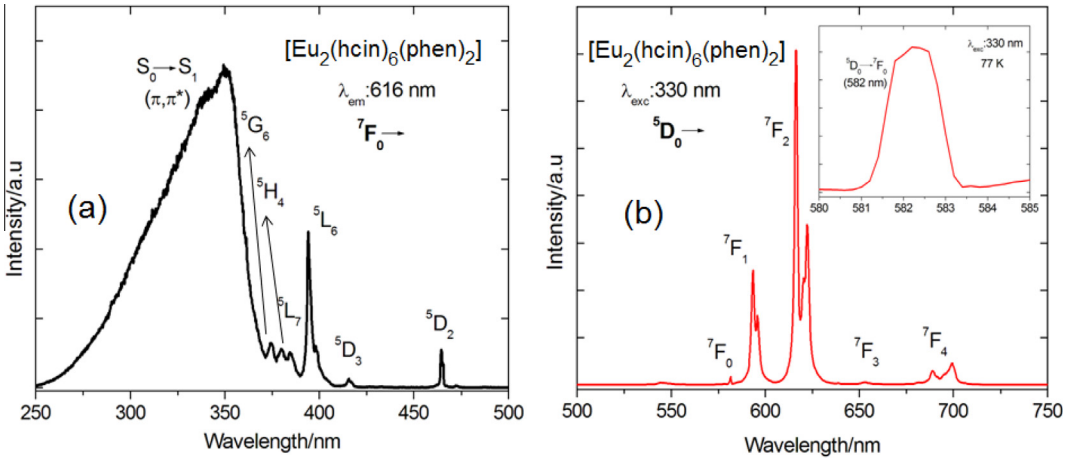

Fig. 5. Photoluminescence excitation (a) and emission (b) spectra for *[Eu₂(hcin)₆(phen)₂]* **1**. Excitation spectrum was obtained for the emission maxima, while the emission spectrum was monitored on the ligands band, at 330 nm.

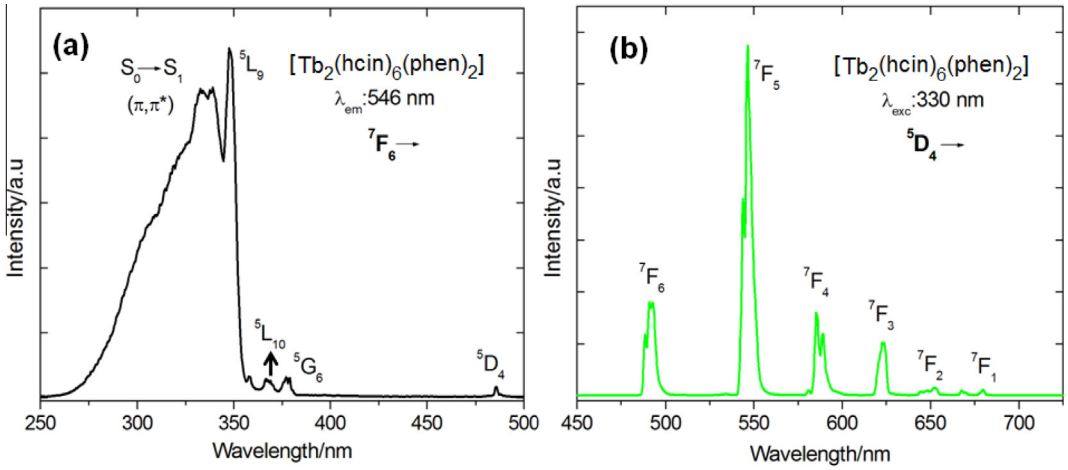

Fig. 6. Photoluminescence excitation (a) and emission spectra (b) for *[Tb₂(hcin)₆(phen)₂]* **3**. Excitation spectrum was obtained at emission maximum, while the emission spectrum was obtained in the solid state, upon excitation at 330 nm.

provides. This transition (582 nm) consists of only one peak, which gives a strong indication that the Eu(III) ions experience the same crystal-field strength and occupy sites of same symmetry. To confirm these results, an emission spectrum in $^5D_0 \rightarrow {}^7F_0$ region was obtained at 77 K (inset in Fig. 7b), and no splitting of this band was observed, corroborating with the crystallographic data. Additionally, a prominent feature that may be observed in this spectrum is the high intensity of $^5D_0 \rightarrow {}^7F_2$ transition, which indicates that a highly polarizable chemical environment around the Eu (III) ion of this complex was responsible for the strong brilliant red emission.

Fig. 6a shows the excitation spectrum of the *[Tb₂(hcin)₆(phen)₂]* **3** complex recorded at 303 K in the 250–500 range, monitoring the emission from the $^5D_4 \rightarrow {}^7F_5$ transition at around 546 nm. As shown in Fig. 6a, a broad band was noted between 250 and 345 nm, which was assigned to intraligand transitions. Several Laporte-forbidden *f–f* transition bands at 355–500 nm range, corresponding to characteristic transitions of Tb(III) ion can be noticed. These bands were assigned to $^7F_6 \rightarrow {}^5L_9$ (353 nm), $^7F_6 \rightarrow {}^5L_{10}$ (367 nm), $^7F_6 \rightarrow {}^5G_6$ (378 nm) and $^7F_6 \rightarrow {}^5D_4$ (485 nm) transitions. Complex **3** exhibits several characteristic emission bands upon excitation in the ligand absorption band, at 330 nm (Fig. 6b). The emission spectrum is composed of the typical Tb (III) green emission, corresponding to $^5D_4 \rightarrow {}^7F_6$ (488 and 491 nm), $^5D_4 \rightarrow {}^7F_5$ (543 and 546 nm), $^5D_4 \rightarrow {}^7F_4$ (583, 585 and 589 nm), $^5D_4 \rightarrow {}^7F_3$ (623 nm), $^5D_4 \rightarrow {}^7F_2$ (644, 648 and 652 nm) and $^5D_4 \rightarrow {}^7F_1$ (685 nm). The compound was also excited in the intense transition ($^7F_6 \rightarrow {}^5L_9$ transition), but no difference in *4f–4f* transitions profile was observed, indicating that the same emission mechanism takes place. These results suggest a high photoluminescence emission of complex **3** when excited directly at the Tb (III) ion, unlike the complex *[Eu₂(hcin)₆(phen)₂]* **(1)** where the sensitization through the ligands is more efficient.

One of factors that governs the luminescence efficiency of lanthanide complexes is the energy-level match between the ligand triplet states and Ln(III) ion ^5D_J state. Thus, the back energy-transfer process is one of the major mechanism of luminescence quenching in Tb(III) complexes. In this context, Latva's empirical rule states [47] show that an efficient ligand-to-metal energy transfer process for Ln(III) needs $\Delta E(^3\pi\pi^* - c^5D_J) > 2000\ cm^{-1}$ for Tb(III). In complex **3**, the energy gap, $\Delta E(^3\pi\pi^* - c^5D_4)$ is lower ($1798\ cm^{-1}$) than the optimal value, however the ligand-to-metal energy transfer process is still effective, despite the back energy transfer between $^5D_4$ levels of Tb(III) ion and $^3\pi\pi^*$. Marques et al. recently reported the *[Tb₂(hcin)₆(bpy)₂]* [20] complex, in which the energy gap is $2173\ cm^{-1}$, and thus the back energy-transfer process has no significant importance in this compound. The smallest energy gap in *[Tb₂(hcin)₆(phen)₂]* compound, studied here, can

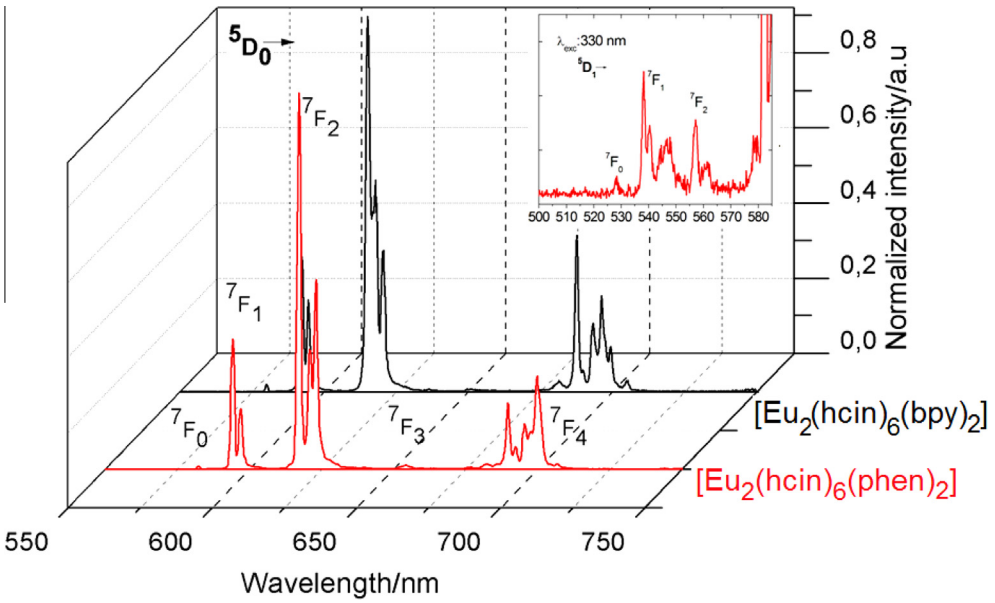

Fig. 7. (a) Normalized emission spectra of *[Eu₂(hcin)₆(bpy)₂]* [20] *and [Eu₂(hcin)₆(phen)₂]* **1** in the solid state at 77 K, upon excitation at 310 and 330 nm, respectively. (Inset: the transitions from $^5D_1$ excited state to $^7F_0$, $^7F_1$ and $^7F_2$ states in the complex **1**).

be explained checking triplet states energy: 22,172 cm^{-1} in *[Gd₂(hcin)₆(phen)₂]* and 22,573 cm^{-1} in *[Gd₂(hcin)₆(bpy)₂]* [20]. In order to get further information on the Eu(III) ion chemical environment for the *[Eu₂(hcin)₆(phen)₂]* **1** complex, the experimental Ω_2 and Ω_4 intensity parameters were determined. According to the theory model developed for the *4f–4f* transitions, the calculus to obtain the intensity parameters (Ω_2 and Ω_4), called Judd–Ofelt parameters, are determined through the transition band intensities of the $^5D_0$ to the ^7F_J ($J = 2$ and 4) levels. The luminescence intensity (I) of the Eu(III) ion transitions is given by Eq. (1):

$$I_{0\to J} = \hbar\omega_{0J} \cdot A_{0\to J} \cdot N_0 = S_{0\to J} \tag{1}$$

where $A_{0\to J}$ is the Einstein spontaneous emission coefficient, N_0 is the population of the emitter level ($^5D_0$), and $\hbar\omega_{0J}$ is the transition energy. $A_{0\to J}$ is the Einstein spontaneous emission coefficient (for the $^5D_0 \to {}^7F_2$ and $^5D_0 \to {}^7F_4$ electronic transitions). For $A_{0\to J}$ calculation, the bellow equation is considered [48]:

$$A_{0\to J} = \frac{\sigma_{0\to 1}}{S_{0\to 1}} \cdot \frac{S_{0\to J}}{\sigma_{0\to J}} . A_{0\to 1} \tag{2}$$

where $\sigma_{0\to 1}$ and $\sigma_{0\to J}$ correspond to energy baricenters of $^5D_0 \to {}^7F_1$ and $^5D_0 \to {}^7F_J$, respectively. $S_{0\to 1}$ and $\S_{0\to J}$ are emission curve areas corresponding to $^5D_0 \to {}^7F_1$ and $^5D_0 \to {}^7F_J$ transitions, respectively [49]. As known, the magnetic dipole allowed $^5D_0 \to {}^7F_1$ transition was taken as reference [50], since $A_{0\to 1}$ rate is almost insensitive to chemical environment changes around the Eu(III) ion with $A_{0\to 1} \cong 50 s^{-1}$. The experimental intensity parameters Ω_λ ($\lambda = 2$ and 4) are estimated from the $^5D_0 \to {}^7F_2$ and $^5D_0 \to {}^7F_4$ transitions, respectively, in the emission spectrum of the Eu(III) complex. The experimental intensities parameters were calculated from the spontaneous emission coefficients ($A_{0\to J}$), according to the following expression [51]:

$$\Omega_\lambda = \frac{3\hbar c^3 A_{0\to J}}{4e^2\omega^3\chi < {}^7F_J \| U^{(\lambda)} \| {}^5D_0 >^2} \tag{3}$$

where χ is the Lorentz local field correction term, given by $\chi = \frac{n(n+2)^2}{9}$ and $< {}^7F_J \| U^{(\lambda)} \| {}^5D_0 >^2$ is a squared reduced matrix element with value of 0.0032 for the $^5D_0 \to {}^7F_2$ transition and 0.0023 for the $^5D_0 \to {}^7F_4$ one and Ω_λ are the Judd–Ofelt intensity parameters [52,53]. The refraction index (n) has been assumed equal to 1.5. In this work, the $^5D_0 \to {}^7F_6$ transition was not observed experimentally; consequently, the experimental Ω_6 parameter could not be estimated. In particular, Ω_2 is more sensitive to symmetry and sequence of ligands fields. Based on the emission spectrum and lifetime of $^5D_0$ emitting level, the emission quantum efficiency (η) of europium ion in compound *[Eu₂(hcin)₆(phen)₂]* **1** was determined. Initially the emission coefficients A_{02} and A_{04} corresponding to $^5D_0 \to {}^7F_2$ and $^5D_0 \to {}^7F_4$ transitions, respectively, were calculated according to the Eq. (2). Considering the ratio between the emitting state lifetime and total decay rate, ($A_{total} = 1/\tau = A_{rad} + A_{nrad}$), the η value can be calculated by the Eq. (4) [54]:

$$\eta = \frac{A_{rad}}{A_{rad} + A_{nrad}} \tag{4}$$

The values of spectroscopic properties as Ω_λ intensity parameters ($\lambda = 2$ and 4), radiative (A_{rad}) and nonradiative (A_{nrad}) decay rates, luminescence lifetimes (τ) and quantum efficiency (η) of *[Eu₂(hcin)₆(phen)₂]* **1** complex, together with those for complex *[Eu₂(hcin)₆(bpy)₂]* [20] are shown in Table 4. The signal intensities of these complexes are compared in Fig. 7. Additionally, from the comparison between the emission spectra obtained at 300

Table 4
Photoluminescence data of *[Eu₂(hcin)₆(phen)₂]* **1** complex and *[Eu₂(hcin)₆(bpy)₂]* [20] complex, both in the solid state.

Eu(III) complexes	Ω_2 (10^{-20} cm^2)	Ω_4 (10^{-20} cm^2)	A_{rad} (s^{-1})	A_{nrad} (s^{-1})	A_{total} (s^{-1})	τ (ms)	η (%)
[Eu₂(hcin)₆(phen)₂]	7.91	8.33	383.5	145.6	529.1	1.89[a]	72
[Eu₂(hcin)₆(bpy)₂] Ref. [20]	7.17	8.96	412.5	204.7	617.2	1.62[a]	67

[a] Error: ±0.001 ms.

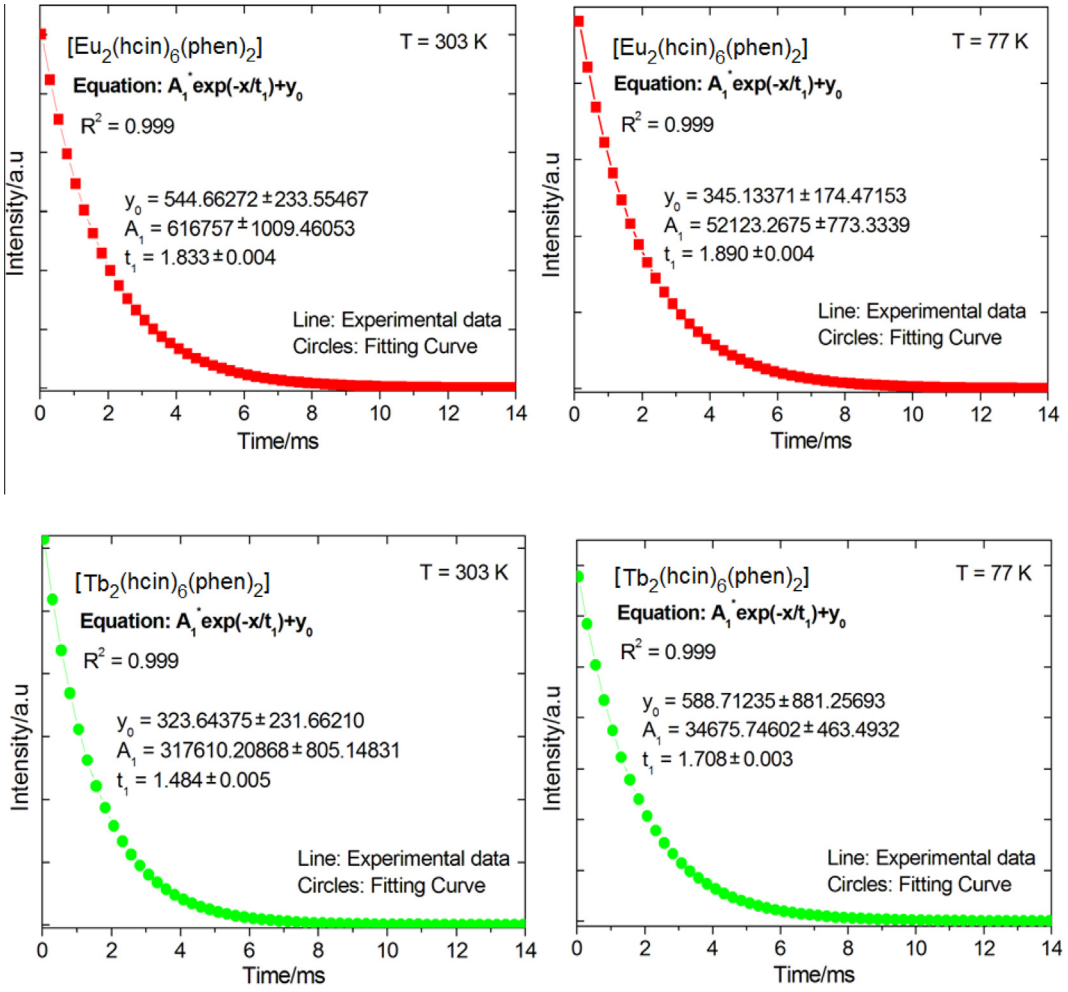

Fig. 8. Typical luminescence decay profiles observed for *[Eu$_2$(hcin)$_6$(phen)$_2$]* **1** and *[Tb$_2$(hcin)$_6$(phen)$_2$]* **3** in the solid state at low temperature (77 K) and room temperature (303 K), with excitation at 330 nm.

(Fig. 5b) and 77 K (Fig. 7), a better resolution of spectral lines at low temperature with significant difference due to Stark levels was observed. In this spectrum the transitions from $^5D_1$ excited state to $^7F_0$, $^7F_1$ and $^7F_2$ states can be also observed (inset in Fig. 9). Such transitions exhibit extremely low intensity because $^5D_0$ and $^5D_1$ levels have small energy gap, and so, the energy transfer $^5D_1 \rightarrow {}^5D_0$ is preferred in relation to electronic transitions $^5D_1 \rightarrow {}^7F_J$ (J = 0–6).

The intensity parameters values (Ω_2 and Ω_4) for the *[Eu$_2$(hcin)$_6$(phen)$_2$]* complex are similar to those found for *[Eu$_2$(hcin)$_6$(bpy)$_2$]* complex (Table 4) leading to the conclusion that the local geometry and the ligating atoms polarizabilities are relatively similar in both complexes. The Ω_4 parameter is influenced by the ion–ligand and ion–ion bond distances. The smaller emitter ions distance the greater the value Ω_4, indicating that there are long-range interactions between luminescent ions. In *[Eu$_2$(hcin)$_6$(phen)$_2$]* complex the Eu···Eu distance of 4.063 Å is slightly larger than the Eu···Eu distance of 3.951 Å in *[Eu$_2$(hcin)$_6$(bpy)$_2$]*. These values are consistent with those Ω_4 values found for the complexes: 8.33 for the *[Eu$_2$(hcin)$_6$(phen)$_2$]* and 8.96 for the *[Eu$_2$(hcin)$_6$(bpy)$_2$]*. The $^5D_0 \rightarrow {}^7F_0$ transition energy can be correlated with the covalence degree of Eu–L bonds and the red shift of this transition is due to the nephelauxetic effect [55–57]. In order to promote a comparison between *[Eu$_2$(hcin)$_6$(bpy)$_2$]* and *[Eu$_2$(hcin)$_6$(phen)$_2$]* complexes, the $^5D_0 \rightarrow {}^7F_0$ transition centroid energy was determined and these values are: 580 nm (17,241 cm^{-1}) for *[Eu$_2$(cin)$_6$(bpy)$_2$]* complex and

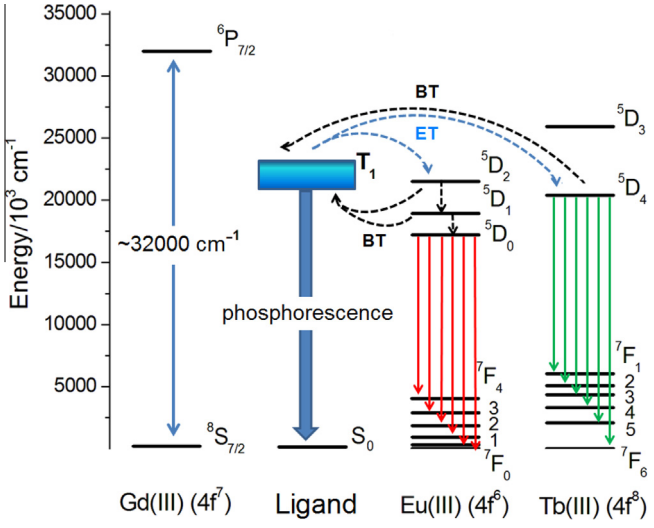

Fig. 9. Schematic energy level diagram and the possible energy transfer process in the systems of *[Eu$_2$(hcin)$_6$(phen)$_2$]* **1** and *[Tb$_2$(hcin)$_6$(phen)$_2$]* **3.** T_1, the first excited triplet state; BT, back-energy transfer; ET, energy transfer.

582 nm (17,182 cm^{-1}) for *[Eu$_2$(hcin)$_6$(phen)$_2$]* **1** (Fig. S6 in Supplementary Material). These results indicate that the complexes covalence depends on the ancillary ligand nature, being higher for

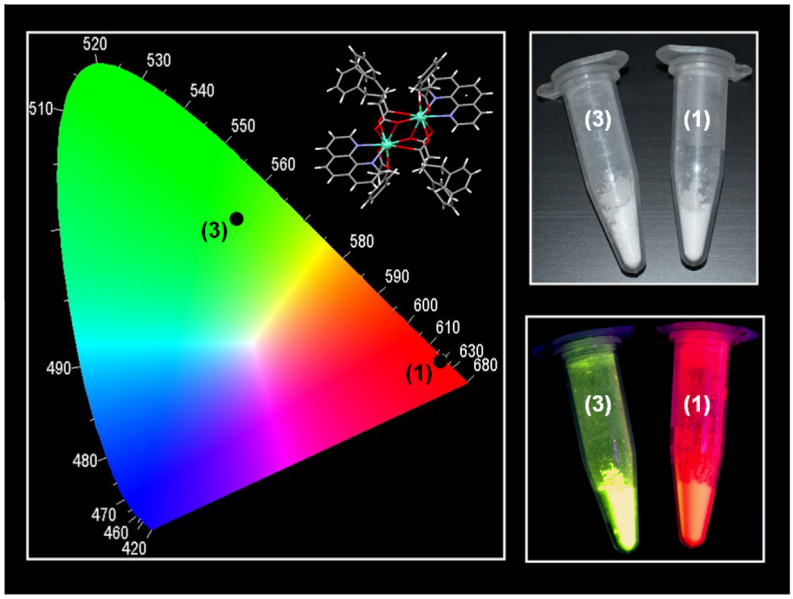

Fig. 10. Left: CIE chromaticity diagram showing the (*x*,*y*) emission color coordinates for *[Ln$_2$(hcin)$_6$(phen)$_2$]* complexes (where: Ln = Eu (III) and Tb(III)). Right: Photographs of complexes (with a digital camera) displaying the intense photoluminescence in red and green regions, respectively, under UV irradiation at 330 nm. (For interpretation of the references to colour in this figure legend, the reader is referred to the web version of this article.)

L = 1,10 phenanthroline (phen) than for 2,2′-bipyridine (bpy), although both complexes present close Ω_2 intensity parameters values. Similar results were reported for *[Eu(Et$_2$NCS$_2$)$_3$bpy]* and *[Eu(Et$_2$NCS$_2$)$_3$phen]* complexes [58] and for several other complexes in chloroformic solutions [59]. Complexes **1** and **3** luminescence lifetimes (τ) in the solid state have been determined at 300 and 77 K, under excitation at 330 nm, with emission monitored at $^5D_0 \rightarrow {}^7F_2$ and $^5D_4 \rightarrow {}^7F_5$ transitions for Eu(III) and Tb(III), respectively. Each of the decay curves (Fig. 8) follows monoexponential decay law, and the equation intensity = $A_1.\exp(-x/t_1) + y_0$ was used for fitting the fluorescence decay curves.

These data are also consistent with only one symmetry site for both complexes, in agreement with Eu(III) complex emission spectrum and X-ray diffraction analysis. The lifetimes values, at 303 K, are 1.83 ms for *[Eu$_2$(hcin)$_6$(phen)$_2$]* **1** and 1.48 ms for *[Tb$_2$(hcin)$_6$(phen)$_2$]* **3**,and at liquid nitrogen temperature (77 K) are greater, 1.89 and 1.70 ms, respectively. This fact is related to the decrease in vibrational contributions caused by the decrease in the temperature. As expected, the highest lifetime values obtained for the compounds are due the absence of water in first coordination sphere, in accordance with FTIR and thermal analysis data. The emission lifetime value for the *[Eu$_2$(hcin)$_6$(phen)$_2$]* **1** complex (τ = 1.89 ms) is greater than the value obtained for the *[Eu$_2$(hcin)$_6$(bpy)$_2$]* (τ = 1.62 ms) [20], reflecting on a greater quantum efficiency (η) value for complex **1**, containing phen ligand. The stronger luminescence observed for *[Eu$_2$(hcin)$_6$(phen)$_2$]* can be associated to a greater structural rigidity of phen ligand, allowing a better energy transfer. The rigid structure restricts the thermal vibration of the ligand and reduces the energy loss by radiationless decay. Yang et al. [60] reported similar fact, comparing a more intense emission for *[Eu(tta)$_3$(phen)]* than for *[Eu(tta)$_3$(bpy)]*. Also, the optimum energy gap between the triplet (T_1) energy levels and $^5D_{0,1}$ states in *[Eu$_2$(hcin)$_6$(phen)$_2$]* complex in relation to the *[Eu$_2$(hcin)$_6$(bpy)$_2$]* complex (according to the phosphorescence spectra) provides high values of intramolecular energy transfer minimizing the back-energy transfer process. According to the above experimental results, the schematic energy level diagram and the most probable channels for the intramolecular energy transfer process are shown in Fig. 9.

The *[Ln$_2$(hcin)$_6$(phen)$_2$]* (Ln = Eu **(1)** and Tb **(3)**) complexes show (*x*,*y*) color coordinates for Eu(III) (0.689, 0.308) and Tb(III) (0.323, 0.557) in the red and green regions of the CIE chromaticity diagram (*Commission Internationale de l'Eclairage*), respectively, as exhibited in Fig. 10. Therefore, these complexes act as light conversion molecular devices (LCMDs) producing intense monochromatic emission colors and can be applied in bicolor devices.

4. Conclusions

In this work, new binuclear complexes of lanthanide ions with the hydrocinnamate ligand are presented. The complexes, of general formula *[Eu$_2$(hcin)$_6$(phen)$_2$]*, (Ln = Eu **1**; Gd **2**; Tb **3**; hcin = hydrocinnamate anion; phen = 1,10-phenanthroline) were synthesized, fully characterized and their photophysical properties were studied in detail. The crystal structures of complexes were solved and refined using powder X-ray diffraction patterns, revealing that all compounds are isostructural and that each lanthanide ion is nine coordinated by oxygen and nitrogen atoms to form distorted tricapped trigonal-prismatic coordination polyhedron. According to the photoluminescence study, the phosphorescence broad bands from ligands are not present in any spectra, which suggest that the intramolecular ligand-to-metal energy transfer is efficient. This fact was reinforced by measuring the first triplet state (T_1) energies of the organic ligands that is above $^5D_0$ Eu(III) and $^5D_4$ Tb(III) energy levels. The values of spectroscopic properties as Ω_λ intensity parameters (λ = 2 and 4), radiative (A_{rad}) and nonradiative (A_{nrad}) decay rates, luminescence lifetimes (τ) and quantum efficiency (η) of *[Eu$_2$(hcin)$_6$(phen)$_2$]* **1** complex was calculated from the experimental data and compared to those values for the similar complex *[Eu$_2$(hcin)$_6$(bpy)$_2$]* previously reported. The *[Eu$_2$(hcin)$_6$(phen)$_2$]* **1** displays a quantum yield about 73% suggesting that the system can act as efficient light-conversion molecular devices (LCMDs). According to our studies in the binuclear hydrocinnamates, the phen ligand could be a better candidate on sensitizing Eu(III) ion luminescence than bpy ligand. These results have motivated us to synthesize and develop new highly photoluminescent binuclear hydrocinnamates of lanthanides given a scarcity of these

compounds in the literature. This class of compounds has shown great promise in the development of electroluminescent devices.

Acknowledgments

The authors thank the Brazilian agencies CNPq (304657/2013-1), CAPES, FAPESP and FAPEMIG (CEX-APQ 00808-13). The authors are also very grateful to Dr. Luiz Fernando Brum Malta (Instituto de Química da Universidade Federal do Rio de Janeiro) for thermal analysis measurements.

Appendix A. Supplementary material

CCDC 1420383–1420385 contain the supplementary crystallographic data for the compound **1**–**3**. These data can be obtained free of charge from The Cambridge Crystallographic Data Centre via www.ccdc.cam.ac.uk/data_request/cif. Supplementary data associated with this article can be found, in the online version, at http://dx.doi.org/10.1016/j.ica.2015.11.009.

References

[1] J.C.G. Bünzli, G.R. Choppin (Eds.), Lanthanide Probes in Life, Chemical and Earth Sciences – Theory and Practice, Elsevier, Amsterdam, 1989 (Chapter 7).
[2] F.S. Richardson, Chem. Rev. 82 (1982) 541.
[3] H. Mikola, H. Takalo, I. Hemmila, Bioconjug. Chem. 6 (1995) 235.
[4] J. Rocha, L.D. Carlos, F.A.A. Paz, D. Ananias, Chem. Soc. Rev. 40 (2011) 926.
[5] M.A. Katkova, T.V. Balashova, V.A. Ilichev, A.N. Konev, N.A. Isachenkov, G.K. Fukin, S.Y. Ketkov, M.N. Bochkarev, Inorg. Chem. 49 (2010) 5094.
[6] M.G. Lahoud, L.F. Marques, P.B. Silva, C.A. Jesus, C.C. Silva, J.A. Ellena, R.S. Freitas, M.R. Davolos, R.G.C. Frem, Polyhedron 54 (2013) 1.
[7] D. Parker, Aust. J. Chem. 64 (2011) 239.
[8] L.F. Marques, C.C. Correa, S.J.L. Ribeiro, M.V. dos Santos, J.D.L. Dutra, R.O. Freire, F.C. Machado, J. Solid State Chem. 227 (2015) 68.
[9] N. Sabbatini, M. Guardigli, J.M. Lehn, Coord. Chem. Rev. 123 (1993) 201.
[10] G. Zucchi, V. Murugesan, D. Tondelier, D. Aldakov, T. Jeon, F. Yang, P. Thuery, M. Ephritikhine, B. Geffroy, Inorg. Chem. 50 (2011) 4851.
[11] H.F. Li, P.F. Yan, P. Chen, Y. Wang, H. Xu, G.M. Li, Dalton Trans. 41 (2012) 900.
[12] Y. Wang, Y. Song, Z.R. Pan, Y.Z. Shen, Z. Hu, Z.J. Guo, H.G. Zheng, Dalton Trans. 41 (2008) 5588.
[13] L.F. Marques, M.V. dos Santos, S.J.L. Ribeiro, E.E. Castellano, F.C. Machado, Polyhedron 38 (2012) 149.
[14] C. Daiguebonne, N. Kerbellec, G. Ouillou, J.C. Bunzli, F. Gumy, L. Catala, T. Mallah, A. Nudebrand, Y. Gerault, K. Bernot, G. Calvez, Inorg. Chem. 47 (2008) 3700.
[15] C.W. Moss, M.A. Lambert, D.J. Goldsmith, Appl. Microbiol. 19 (2) (1970) 375.
[16] S.M. Korneev, Synthesis 45 (8) (2013) 1000.
[17] R. Najjar, W. de Oliveira, J.B. Carducci, Polyhedron 8 (1989) 1157.
[18] E. Dubler, U.K. Haring, K.H. Scheller, P.H. Baltzer, Inorg. Chem. 23 (1984) 3785.
[19] L.F. Marques, A.A.B.C. Junior, C.C. Correa, M.G. Lahoud, R.R. da Silva, S.J.L. Ribeiro, F.C. Machado, J. Photochem. Photobiol. A: Chem. 252 (2013) 69.
[20] L.F. Marques, C.C. Correa, H.C. Garcia, S.J.L. Ribeiro, J.D.L. Dutra, R.O. Freire, F.C. Machado, J. Lumin. 148 (2014) 307.
[21] S. Biju, D.B. Ambili, M.L.P. Reddy, B.M. Kariuki, Inorg. Chem. 45 (2006) 10651.
[22] W.J. Chai, W.X. Lin, X.J. Sun, T. Ren, X.Y. Shi, J. Lumin. 131 (2011) 225.
[23] A.A. Coelho, J. Appl. Crystallogr. 36 (2003) 86.
[24] TOPAS-R (2009). Version 4.2, General profile and structure analysis software for powder diffraction data, Bruker AXS, Karlsruhe, Germany.
[25] G.S. Pawley, J. Appl. Crystallogr. 14 (1981) 357.
[26] A. Coelho, J. Appl. Crystallogr. 22 (2000) 899.
[27] A.L. Spek, Acta Crystallogr. D65 (2009) 148.
[28] Y.V. Nelyubina, A.A. Korlyukov, K.A. Lyssenko, Mendeleev Commun. 24 (2014) 286.
[29] U. Das, B. Chattopadhyay, M. Mukherjee, A.K. Mukherjee, Cryst. Growth Des. 12 (2012) 466.
[30] R.A. Young, "The Rietveld Method", IUCr Monograph N.5 Oxford University Press, New York, 1981.
[31] S.A. da Silva, C.Q.F. Leite, F.R. Pavan, N. Masciocchi, A. Cuin, Polyhedron 79 (2014) 170.
[32] S.A. da Silva, N. Masciocchi, A. Cuin, Powder Diffr. 29 (3) (2014) 300.
[33] T.C. Amaral, G.S.G. Carvalho, A.D. da Silva, P.P. Corbi, N. Masciocchi, E.E. Castellano, A. Cuin, J. Coord. Chem. 67 (8) (2014) 1380.
[34] N. Masciocchi, A. Sironi, J. Chem. Soc., Dalton Trans. (1997) 4643.
[35] E. Keller, Chem. unserer Zeit 20 (1986) 178.
[36] G.B. Deacon, C.M. Forsyth, P.C. Junk, M. Hilder, S.G. Leary, C. Bromant, I. Pantenburg, G. Meyer, B.W. Skelton, A.H. White, Z. Anorg. Allg. Chem. 634 (2007) 91.
[37] A. de Bettencourt-Dias, S. Viswanathan, Dalton Trans. 34 (2006) 4093.
[38] X. Li, Y.Q. Zou, B. Zheng, H.M. Hu, Acta Crystallogr., Sect. C 60 (2004) 197–199.
[39] L.-Z. Cai, W.-T. Chen, M.-S. Wang, G.-C. Guo, J.-S. Huang, Inorg. Chem. Commun. 7 (2004) 611.
[40] G.B. Deacon, R.J. Phillips, Coord. Chem. Rev. 33 (1980) 227.
[41] J. Vícha, C. Foroutan-Nejad, T. Pawlak, M.L. Munzarová, M. Straka, R. Marek, J. Chem. Theory Comput. 11 (2015) 1509.
[42] S. Aime, I. Bertini, C. Luchinat, Coord. Chem. Rev. 150 (1996) 221.
[43] R.J. Smernik, J.M. Oades, J. Environ. Qual. 31 (2002) 414.
[44] S. Tobita, M. Arakawa, I. Tanaka, J. Phys. Chem. 89 (1985) 5649.
[45] S. Tobita, M. Arakawa, I. Tanaka, J. Phys. Chem. 88 (1984) 2697.
[46] P. A. Tanner, in Lanthanide Luminescence. Photophysical, Analytical and Biological Aspects, ed. P. Hanninen and H. Harma, Springer, Berlin, 2011, ch. 7, pp. 183–233.
[47] M. Latva, H. Takalo, V.M. Mukkala, C. Matachescu, J.C. Rodriguez-Ubis, J. Kanakare, J. Lumin. 75 (1997) 149.
[48] C.D. Donegá, S. Alves Jr., G.F. de Sá, J. Alloys Compd. 250 (1997) 422–426. Lausanne.
[49] E.E.S. Teotonio, G.M. Fett, H.F. Brito, W.M. Faustino, G.F. de Sa, M.C.F.C. Felinto, R.H.A. Santos, J. Lumin. 128 (2008) 190.
[50] D.B. Ambili, S. Raj, M.L.P. Biju, Inorg. Chem. 47 (2008) 8091.
[51] O.L. Malta, H.F. Brito, J.F.S. Menezes, J. Lumin. 75 (1997) 255.
[52] B.R. Judd, Phys. Rev. 127 (1962) 750.
[53] G.S. Ofelt, J. Chem. Phys. 37 (1962) 511.
[54] G.F. de Sá, O.L. Malta, C.M. Donegá, A.M. Simas, R.L. Longo, P.A. Santa-Cruz, E.F. da Silva Jr., Coord. Chem. Rev. 196 (2000) 165–195.
[55] O.L. Malta, H.J. Batista, L.D. Carlos, Chem. Phys. 282 (2002) 21.
[56] R.A.S. Ferreira, S.S. Nobre, C.M. Granadeiro, H.I.S. Nogueira, L.D. Carlos, O.L. Malta, J. Lumin. 121 (2006) 561.
[57] A.P. Souza, L.C.V. Rodrigues, H.F. Brito, S. Alves Jr., O.L. Malta, J. Lumin. 130 (2010) 181.
[58] W.M. Faustino, O.L. Malta, E.E.S. Teotônio, H.F. Brito, A.M. Simas, G.F. de Sá, J. Phys. Chem. A 110 (2006) 2510.
[59] C.Y. Su, M.Y. Tan, N. Tang, W. Liu, X. Wang, J. Coord. Chem. 38 (1996) 207.
[60] Y.S. Yang, M.L. Gong, Y.Y. Li, H.Y. Lei, S.L. Wu, J. Alloys Compd. 112 (1994) 207.